PHYSICAL REVIEW B VOLUME 8, NUMBER 10 15 NOVEMBER 1973

Effect of Free Carriers on Zone-Center Vibrational Modes in Heavily Doped *p*-type Si. II. Optical Modes

Fernando Cerdeira, T. A. Fjeldly, and M. Cardona
Max-Planck-Institut für Festkörperforschung, Stuttgart, Bundesrepublik Deutschland
(Received 11 June 1973)

The effect of free holes on the optical phonons of Si at the zone center is investigated with Raman scattering. The presence of holes produces an inter-valence-band, electronic, broad, scattering background which overlaps with the one-phonon Raman line. This overlap results in a Fano-type continuous-discrete interference. The parameters Γ and q of the resulting Fano scattering line can be varied by changing (a) the laser wavelength and (b) the free-carrier concentration. A theoretical interpretation of these results based on the detailed valence-band structure of Si and on the resonant characteristics of the vibronic and electronic Raman scattering is presented. The effect of uniaxial stress on this composite Raman scattering of *p*-type Si is also investigated. At large stresses the electronic background disappears and the phonon lines recover the linewidths of the intrinsic material. The behavior in the intermediate-stress range is very similar to that reported for the acoustical phonons in the previous paper.

I. INTRODUCTION

Heavy acceptor doping is known to affect the position and width of the one-phonon Raman lines of Ge and Si.[1] The observed effects in Ge can be successfully explained with the same type of model used to describe the effects of carrier concentration on the elastic constants of the material.[1–3] Here the phonon is considered as a "static" perturbation (i.e., the phonon frequency is considered small with respect to the separation between relevant electronic energy states) which splits the top of the valence band and causes the dispersion relation of the holes to change. These modifications in the band structure lead to interband and intraband redistribution of carriers, which lowers the electronic contribution to the free energy of the crystal. In this way part of the energy spent in deforming the crystal is regained through carrier redistribution with a consequent "softening" of the crystal with respect to that particular vibration. This "softening" is translated into a shift of the phonon frequency towards lower energies observed in the Raman spectrum.[1] The isotropic broadening of the Raman line is explained phenomenologically when the finite redistribution time of carriers is taken into account.[1] In this way, the effects of heavy acceptor doping on the Raman frequency and C_{44} elastic constant of Ge were quantitatively explained and both effects were shown to be intimately related to each other.[1] The same type of model gives a satisfactory account of the carrier-induced changes in the C_{44} elastic constant of *p*-type Si.[3] The Raman spectrum of this material, however, shows several puzzling characteristics which have no analog in the associated elastic constants. In contrast to Ge, the broadening produced by the carriers in the Raman spectrum of Si is asymmetric and has strong dependence on the frequency of the incoming light.[4,5] In a preliminary report of this work[5] we proposed an explanation based on a discrete-continuum Fano-type[6] interaction between the one-phonon scattering and one-electron excitations from filled to empty valence states. These excitations are infrared forbidden[7] but Raman allowed at $\vec{k}=0$ because of parity and thus provide a scattering mechanism which spreads over a continuum whose energy overlaps with that of the one-phonon scattering. The resulting line shape is produced by the interference between the discrete and continuum scattering mechanisms.[5,6] In this paper we make a systematic study of the Raman spectrum of *p*-type Si for a wide range of carrier concentrations, at different scattering frequencies. The explanation proposed in Ref. 5 is thus shown to be generally valid and to give good account of all the observed phenomena. From the fitting of the experimental data with the Fano line shape, two wavelength-independent parameters are obtained which represent the real and imaginary parts of the phonon self-energy.[5] The carriers are shown to decrease the phonon energy and to increase its natural linewidth. These effects are similar to those observed in Ge,[1] and a relationship could now be drawn between changes in phonon energy and width with the changes in elastic constants discussed in the previous paper.[3] In order to investigate this relationship the dependence of phonon energy shift and linewidth on carrier concentration, temperature, and externally applied uniaxial stress is studied and compared with similar measurements on the elastic constants reported on the previous paper.[3] Qualitative analogies are found between the doping-induced changes in C_{44} and phonon self-energies which suggest a close link between these physical quantities. Quantitative understand-

ing of this link would require a more complex theoretical formulation of the electron-phonon problem than is presently available.[1]

II. THEORY

The explanation proposed[5] to account for the observed changes in the Raman spectrum of heavily doped Si with the frequency of the scattering radiation is based on the existence of a continuum of electronic excitations produced by inter-valence-band transitions (see Fig. 1), whose energy overlaps with that of the phonon. These one-electron excitations (infrared forbidden[7] but Raman allowed at $\vec{k}=0$) can also scatter electromagnetic radiation (electronic Raman scattering) giving two competing scattering mechanisms: one produced by the continuum of electronic excitations and another by one-phonon scattering. Owing to the anisotropy of the valence band, the continuum extends from a minimum energy ω_m (equal to the smallest separation between bands at $k=k_F$, which imples $\omega_m \leq \frac{2}{3}\Delta_0$) and extends to very high energies owing to the flatness of the heavy-hole band in certain directions in $\vec{k}$ space (see Fig. 1). Since in Si the spin-orbit splitting Δ_0 is 44 meV while the phonon frequency Ω is about 65 meV, the continuum overlaps in energy with the phonon ($\omega_m < \Omega$) for almost any value of carrier concentration. This would not be true in Ge where $\Delta_0 = 300$ meV and $\hbar\Omega = 37$ meV.

The interaction between discrete and continuum spectra was treated by Fano[6] and is known to lead to asymmetric line shapes of the type observed in the Raman spectrum of p-type Si.[5] We consider here how Fano's theory can be adapted to the case under study. Given a continuum of states ψ_E and

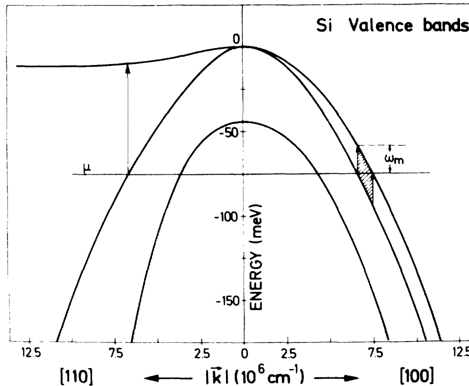

FIG. 1. Valence bands of Si calculated with $\vec{k}\cdot\vec{p}$ effective Hamiltonian as explained in Ref. 3. The vertical arrows show the inter-valence-band transitions of the electronic continuum. The shaded region between arrows corresponds to the total number of transitions for a given direction in $\vec{k}$ space. Here μ stands for Fermi energy and ω_m for the low-energy cutoff of the inter-valence-band continuum.

a discrete state ϕ with overlapping energy, Fano writes the Hamiltonian matrix as[6]

$$\langle\phi|H|\phi\rangle = \hbar\Omega , \quad (1a)$$

$$\langle\psi_E|H|\phi\rangle = V_E , \quad (1b)$$

$$\langle\psi_{E'}|H|\psi_E\rangle = E\,\delta(E-E') , \quad (1c)$$

with $E=\hbar\omega$. This leads to a line shape of the form[6]

$$I(\epsilon, q) = (q+\epsilon)^2/(1+\epsilon^2) , \quad (2a)$$

with

$$\epsilon = (\omega - \Omega - \delta\Omega)/\Gamma . \quad (2b)$$

Here the parameters Γ and q are defined as

$$\hbar\Gamma(\omega) = \pi|V_E|^2 , \quad (3a)$$

$$\Gamma q^2 = \frac{1}{\pi}\frac{|\langle\Phi|T|i\rangle|^2}{|\langle\psi_E|T|i\rangle|^2} , \quad (3b)$$

$$\delta\Omega(\omega) = \frac{1}{\pi}\,\mathcal{P}\int d\omega'\,\frac{\Gamma(\omega')}{\omega-\omega'} , \quad (3c)$$

where $\mathcal{P}$ in Eq. (3c) indicates "principal part of" and T is a transition operator such that the squared matrix element of T gives, in our case, the Raman scattering probability. The states represented by Φ are the discrete states "renormalized" by its interaction with the continuum.[6]

The physical significance of the parameters defined by Eqs. (3) in our case becomes clear. Here $\overline{\Omega} = \Omega + \delta\Omega$ (with $\overline{\Omega}$ and Ω the phonon frequencies in the doped and intrinsic states, respectively) and Γ becomes the real and imaginary part of the phonon self-energy when its interaction with the electronic continuum is taken into account. The parameter Γq^2, being a ratio of transition probabilities, can be written in terms of the Raman tensor for pure electronic, R_e, and pure one-phonon scattering, R_p:

$$\Gamma q^2 \propto |R_p/R_e|^2 . \quad (4)$$

The abstract definition of Γ given in Eq. (3a) can also be translated in terms of our concrete problem in order to obtain numerical estimates for comparison with experiment. First notice that the δ function in Eq. (1c) implies the existence of a true continuum (i.e., infinite number of states). In reality we have a quasicontinuum of electronic excitations with a finite number of states per unit volume given by the difference between the number of carriers in the upper (N_h) and lower (N_l) valence bands. Our quasicontinuum is characterized by a large discrete number of closely spaced states ψ_i. The relation between such states and those defined by Eq. (1c) is given by[8]

$$\psi_E = [\rho(E)V]^{1/2}\psi_i , \quad (5)$$

where $\rho(E)$ is the density of quasicontinuum states

per unit volume and V is the volume of the crystal. Another important difference between Fano's treatment and our problem is that we can have a collection of vastly different ψ_i states for each value of the energy $\hbar\omega$, as we move around in k space over a constant energy surface. This multiplicity can be approximately taken into account by defining an average matrix element

$$\langle |\langle\psi_i|H|\phi\rangle|^2\rangle_{av} = \frac{1}{\nu_\omega}\sum_{i=1}^{\nu_\omega} |\langle\psi_i|H|\phi\rangle|^2 , \quad (6)$$

where ν_ω is the number of states ψ_i with energy $\hbar\omega$. The parameter Γ can now be written in terms of this "average" matrix element by substituting Eq. (5) into Eqs. (3a) and (1b):

$$\hbar\Gamma(\omega) = \pi\rho(\hbar\omega)\, V\langle|\langle\psi_i|H|\phi\rangle|^2\rangle_{av} . \quad (7)$$

Given the complexity of the band structure of Si, Eq. (7) cannot be evaluated exactly in closed form: It is either numerically computed or calculated under simplifying assumptions. Here we shall make use of some approximations in order to estimate values of Γ and to compare them with our experimental results. We assume Eq. (6) to be independent of the energy $\hbar\omega$ and we perform the average by computing the two-band electron-phonon matrix element in the deformation potential approximation[1,9] for 26 directions in k space (6 $\{100\}$, 8 $\{111\}$, and 12 $\{110\}$), as shown in Appendix A. This leads to the expression (valid for $\mu \gg \frac{2}{3}\Delta_0$)

$$\langle|\langle\psi_i|H|\phi\rangle|^2\rangle_{av} = \tfrac{95}{78}\left(\tfrac{1}{2}\delta E\right)^2 , \quad (8)$$

where δE is the splitting of the top of the valence band produced by the $\vec{k}\simeq 0$ optical phonon. This splitting for the ground state zero-point phonon is given by[9,10]

$$\delta E = \left(\frac{a^3\hbar}{4MV\Omega}\right)^{1/2} \frac{2d_0}{a}\,(1+n_B)^{1/2} , \quad (9)$$

where a is the lattice constant, M the ionic mass, d_0 the corresponding deformation potential[1,9] and n_B is the Bose-Einstein distribution. The expression for Γ thus results:

$$\hbar\Gamma = \frac{\pi}{4}\left(\frac{95}{78}\right)\frac{\hbar a}{M\Omega}\, d_0^2\rho(\hbar\omega)(1+n_B) . \quad (10)$$

In Eq. (10) all the information concerning the carrier-concentration dependence of Γ is to be found in $\rho(\hbar\omega)$. Hence, by inspecting Eqs. (3)-(5) and (10) we observe that the quantity $\Gamma^3 q^2$ should be carrier-concentration independent. The existence of this invariant is experimentally demonstrated in Secs. III and IV. This provides a good test of the validity of the approximations which lead to Eq. (10), in particular, the assumption concerning the energy independence of the average matrix element. In order to obtain numerical estimates of Γ and its dependence on carrier concentration using Eq. (10), we have to obtain a numerical estimate of the combined density of states for the continuum of inter-valence-band transitions. As we shall see later, the experimental data can be excellently fitted with values of Γ independent of the energy $\hbar\omega$. This means that the function $\rho(\hbar\omega)$ is very flat in the neighborhood of $\omega=\Omega$ and has substantial variation only at the flanks of the spectrum [$\omega\to 0$ and $\omega\to\infty$, where $\rho(\hbar\omega)\to 0$]. Hence, we can approximate $\rho(\hbar\omega)$ by its value at the Fermi energy (μ), a value which is relatively easy to calculate. To compute $\rho(\mu)$ we make the further assumption of parabolic bands with masses m_h and m_l for upper and lower valence bands, respectively. Under these assumptions, we obtain

$$\rho(\mu) \simeq \frac{3}{2}\,\frac{\alpha^{3/2}}{(1-\alpha)^{3/2}(1-\alpha^{3/2})}\,\frac{N_h-N_l}{\mu} , \quad (11)$$

where $\alpha = m_l/m_h = 0.32$ taking average effective masses at the top of the valence bands.[11] Here N_h and N_l were defined previously as the number of carriers in the upper and lower valence bands, respectively. With these approximations we obtain

$$\hbar\Gamma \simeq 7.013\times 10^{-2}\left(\frac{\hbar\Omega}{\mu}\right)\frac{d_0^2}{C_{44}^*}(N_h-N_l)(1+n_B) , \quad (12a)$$

where[1,9]

$$C_{44}^* = M\Omega^2/8a = 1.06\times 10^{12}\ \mathrm{erg/cm^3} . \quad (12b)$$

Similar estimates for the change in the real part of the phonon self-energy, $\delta\Omega$, are more difficult to obtain since they depend on the use of Eq. (3c), starting from Eq. (10). In order to do that the behavior of $\rho(\hbar\omega)$ must be known over the whole energy spectrum ($\omega\to\infty$).

III. EXPERIMENT

Our measurements were performed with several lines of an argon-ion and a krypton-ion laser, in the backscattering configuration. A Jarrell-Ash one meter double monochromator with detection by photon counting was used. The frequency of the observed Raman peaks was determined by comparison with several reference lines of a neon low-pressure lamp.

The samples used in this experiment were cut from single-crystal ingots, mechanically polished and chemically etched with a CP-4 solution. The samples for uniaxial stress were aligned by x-ray diffraction to $\pm 1°$ and cut in parallelepipeds of dimensions $1.5\times 1.5\times 17$ mm with the long dimension, that of the applied stress, along the [001] crystallographic direction. The measurements were performed in the configurations $X(Z,Y)\bar{X}$ for the doublet and $X(Y,Y)\bar{X}$ for the singlet phonon. Here, X, Y, and Z represent the $[1\bar{1}0]$, [110],

and [001] directions. The notation used indicates, with the first and last letters, the directions of propagation of the incident and scattered beams, while the first and last letters in parentheses denote the polarization direction (electric field) of incident and scattered radiation, respectively. The selection rules governing this type of scattering are discussed elsewhere.[12,13] The stress apparatus has been extensively described in the literature.[13,14] The low-temperature measurements were performed with the sample immersed in liquid nitrogen for the stress experiments and with the sample placed in a cold finger within an evacuated glass Dewar for the experiments which do not involve the application of stress.

IV. RESULTS AND DISCUSSION

A. Absence of External Stress

The one-phonon Raman spectrum of *p*-type Si was determined for a wide range of carrier concentration starting at 6×10^{18} and up to 4×10^{20} carriers/cm^3, at liquid-nitrogen temperature for two different exciting frequencies ($\lambda = 4880$ Å and $\lambda = 6471$ Å). The resulting line shapes were fitted with the theoretical expression of Eqs. (2) with a least-squares computer fit which used Γ and q as adjustable parameters. Representative samples of this fit are shown in Fig. 2. The fits are in all cases excellent. Notice the pronounced antiresonance at low energies for the 6471 Å excitation wavelength at high carrier concentration, typical of Fano-type line shapes. In particular, in Fig. 2(a), the peak is totally inverted with a sharp antiresonance and flat at high energies. This type of asymmetric "window" line shape has been observed in the x-ray absorption of solidified rare gases[15] and is also associated with discrete-continuum interaction. Evidence of discrete-continuum interaction in the Raman spectrum of $BaTiO_3$ was also presented by Rousseau and Porto[16] where anharmonic interactions between phonon lines lead to line shapes similar to those of Fig. 2. The values of Γ and q resulting from the fit are listed in Table I. The values of $\delta\Omega$ can be obtained by the relations

$$\delta\Omega = \delta\Omega_M - \Gamma/q \ , \tag{13a}$$

$$\delta\Omega = \delta\Omega_m + q\Gamma \ , \tag{13b}$$

which are an immediate consequence of Eqs. (2). Here $\delta\Omega_M$ ($\delta\Omega_m$) is the shift in position of the maximum (minimum) of the doped material spectrum with respect to the one-phonon Raman peak in the intrinsic material. The values thus found for $\delta\Omega$ are also listed in Table I. From this table a number of significant observations can be made.

(a) The values of Γ and $\delta\Omega$ obtained from these fits are, within experimental error, the same for both exciting wavelengths. This confirms our interpretation of these parameters as the real and imaginary part of the change in phonon self-energy owing to electron-phonon interaction. Such quantities should have no relationship with the scatter-

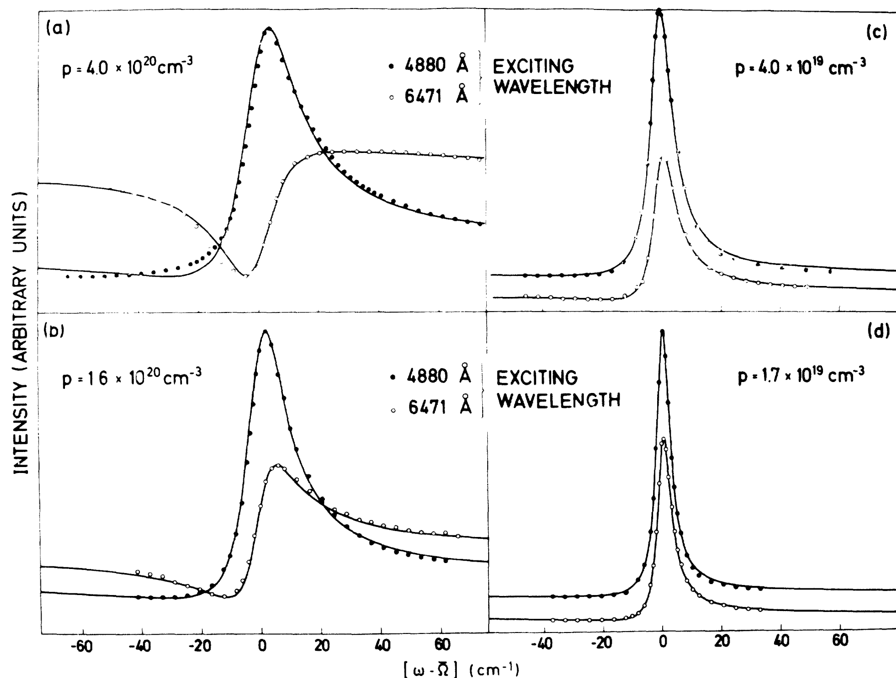

FIG. 2. Raman line shapes for two scattering wavelengths (4880 and 6471 Å). The solid lines are theoretical fits, with Eq. (2), to the experimental curves (discrete points) for different values of the carrier concentration (in cm^{-3}): (a) 4.0×10^{20}, (b) 1.6×10^{20}, (c) 4.0×10^{19}, (d) 1.7×10^{19}. In the last two cases the curves have been shifted vertically with respect to each other, with the antiresonance minimum in each case defining the base line. The relative heights of the two curves for each value of the carrier concentration are the ones found experimentally.

TABLE I. Parameters obtained by fitting experimental first-order Raman spectra of p-type Si at $T=77$ K with the Fano lines shape of Eqs. (2). The spectra were obtained with two different laser lines ($\lambda_L=4880$ and 6471 Å). The values of η are computed for $\lambda_L=4880$ Å.

$10^{-19}N$ (cm^{-3})	q		Γ (cm^{-1})		$\delta\Omega$ (cm^{-1})		$\eta=(\Gamma^3q^2)^{1/5}$ (cm$^{-3/5}$)	$\beta=\frac{q(4880)}{q(6471)}$
	$\lambda_L=4880$ Å	$\lambda_L=6471$ Å	$\lambda_L=4880$ Å	$\lambda_L=6471$ Å	$\lambda_L=4880$ Å	$\lambda_L=6471$ Å		
0.6	32.8	18.4	1.1	1.2	−0.1	−0.1	6.6	1.8
1.7	12.4	6.7	2.8	2.8	−0.4	−0.4	5.0	1.8
2.6	14.6	6.4	3.2	3.2	−0.1	0.0	5.9	2.3
4.0	9.8	4.3	4.4	4.4	−1.1	−1.2	6.0	2.3
7.0	4.7	3.1	6.2	5.9	−1.8	−1.9	5.6	1.5
16	3.7	1.4	8.1	8.1	−6.7	−6.5	5.9	2.6
40	2.8	0.4	10.5	10.7	−14.7	−14.7	6.3	7.0

ing wavelength. This was already suggested in our preliminary study for one value of the carrier concentration as a function of exciting wavelength.[5] The conclusions drawn then[5] are now proven to be correct for a wide range of carrier concentration spanning two decades. We note that $\delta\Omega_M$ and $\delta\Omega_m$ are not independent of scattering wavelength because they are affected by the linewidth of the scattering curves. This is the origin of the anomalies reported in Ref. 4, which, in the context of the present work, appear to be of no relevance.

(b) The parameter q is shown to have a strong dependence on scattering frequency, in line with its definition in Sec. III [see Eq. (4)] as the ratio of the Raman tensor for discrete vibronic and continuum electronic scattering. From Eq. (4) the dependence of q on the exciting frequency can be obtained using the same model for the frequency dependence of both Raman tensors involved. Using the critical point at frequency $\omega_0'=3.3$ eV (E_0' transition at and in the neighborhood of the zone center) as the main source of the dispersive term in both Raman tensors, the relationship

$$q^{-1}\propto \omega_0' - \omega_L , \qquad (14)$$

is obtained,[5] where ω_L is the frequency of the exciting laser. Equation (14) simply follows from the fact that the phonon scattering requires one more intermediate state than the electronic process. Thus, an additional energy denominator results in the phonon scattering. Such an expression is strictly valid only near the energy gap ($\omega_0'=3.3$ eV) but its usefulness was proven[5] on a wider energy range. From Eq. (14) the predicted ratio between q's at 4880- and 6471-Å excitation wavelengths is

$$\beta=q(4880)/q(6471)\simeq 1.83 . \qquad (15)$$

The ratio should be independent of carrier concentration. In Table I the experimental ratios β are listed and they are seen to scatter randomly (i.e., no systematic dependence on carrier concentration is found in accordance with our theoretical considerations) around an average value $\beta=2.0\pm0.6$, in good agreement with Eq. (15). The only significant deviation from this value is shown by one sample with $p=4\times10^{20}$ carriers/cm^3 for which a value $\beta=7.0$ is found. This can be attributed to inhomogeneity in the carrier distribution as we progress from the surface towards the bulk. This inhomogeneity is not unlikely at such high doping levels (close to the solubility limit) and would cause light with different penetration depths to probe regions of different Fermi energies.

In summary, we have proven the validity of describing the one-phonon Raman spectrum of p-type Si as the result of a Fano interaction between the discrete one-phonon scattering and a continuum of electronic scattering. Such an explanation is self-consistent and accounts for the observed line-shape changes with exciting wavelength over a wide range of carrier concentrations.

Now we are in a position to study the changes in phonon energy and linewidth (which, as we proved, are independent of scattering frequency) with carrier concentration. First, we focus our attention on the parameter Γ for which analytic expressions were developed in Sec. II. Let us consider Eq. (7) which was obtained assuming energy independence for the "average-matrix element" and which predicts that the carrier concentration dependence of Γ will arise solely from the density of states $\rho(\hbar\omega)$. As we pointed out in Sec. II, this assumption, together with the definitions of Eqs. (3), (5), and (6) predict the existence of a quantity

$$\eta=(\Gamma^3q^2)^{1/5}$$

which is independent of carrier concentration. The $\frac{1}{5}$ power is taken to preserve the experimental uncertainty. This is confirmed by the values of η

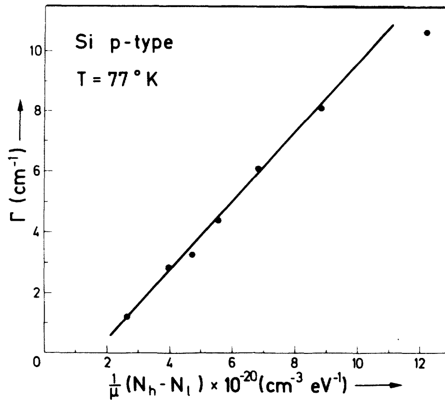

FIG. 3. Parameter Γ from Table I vs model for the joint density of states of Eq. (11). Here N_h and N_l are the number of carriers in the upper and lower valence bands, respectively, and μ stands for the Fermi energy.

listed in Table I which scatter randomly around the value $\eta = 5.9 \pm 0.5$ cm$^{-3/5}$, showing no systematic dependence on carrier concentration. This is convincing evidence of the soundness of the theory presented in Sec. II. Second, let us consider how Γ depends on carrier concentration. This dependence is predicted by Eq. (12) if we rely on the approximation for the density of states given in Eq. (11). This approximation is expected to work well in middle energy ranges (i.e., μ close to $\hbar\Omega$) but will break down at both ends of the energy spectrum ($\mu \ll \hbar\Omega$, $\mu \gg \hbar\Omega$), making Eq. (11) invalid for very high or very low carrier concentrations. In Fig. 3 we show a plot of the values of Γ from Table I versus our model density of states $(N_h - N_l)/\mu$. The partial occupation number of each band and the Fermi energy was calculated from the $\vec{k} \cdot \vec{p}$ bands of Si in the manner described in Ref. 3. Averages $\bar{\Gamma} = \frac{1}{2}[\Gamma(4880) + \Gamma(6471)]$ were taken to improve the statistics, since the small random difference between these two quantities is not significant and can be attributed to statistical error. We see that the experimental points (dots) fall excellently in a straight line, as predicted by Eq. (12), for values of carrier concentration ranging from 6×10^{18} to 1.6×10^{20} cm^{-3}. As expected, deviations start to occur at higher carrier concentrations (4×10^{20} cm^{-3}) due to the breakdown of Eq. (11). The excellent agreement between the theoretical predictions of Eq. (12) for the carrier concentration dependence of Γ and the experimental points illustrated by Fig. 3 provides additional support for the self-consistency of our approach. The comparison of the slope predicted by Eq. (12) (6.9×10^{-20} cm^{-3} eV^{-1}) to the experimental slope of Fig. 3 (1.2×10^{-20} cm^{-3} eV^{-1}) shows that the theoretical expression overestimates the slope by a factor of 5. The theoretical prediction was made by using values of d_0 ($d_0 = 29$ eV) estimated with a pseudopotential approach.[1,9] Since this quantity enters squared in Eq. (12) small deviations in the estimated d_0 from its experimental value would cause large changes in the theoretical slope. Also, we have neglected the strong anisotropy of the Si valence bands and replaced it by spatial "averages." This will contain geometrical factors that could easily introduce factors of 2 or 3 in our estimate of the slope. For instance in Eq. (11) a geometrical factor $\gamma = \frac{3}{2}\alpha^{3/2}[(1-\alpha)^{3/2}(1-\alpha^{3/2})]^{-1}$ appears multiplying $(N_h - N_l)/\mu$ in our estimate of the density of states. Using average values of the masses at the top of the valence band we obtain $\alpha = 0.32$ and $\gamma = 0.59$. Close to the Fermi surface, however, this will give an overestimation of γ, since the light-hole mass increases steadily with increasing k. This alone could easily account for the observed numerical discrepancy between Eq. (12) and experimental Γ's. Because of the uncertainty in the value of these geometrical factors and in d_0 we conclude that Eq. (12) predicts well the functional dependence of Γ on carrier concentration and even gives a fair order of magnitude estimate of the value for this parameter.

It is not so easy to give a quantitative discussion of the carrier-concentration dependence of $\delta\Omega$. In order to obtain theoretical estimates for it the Kramers-Kronig transform of $\Gamma(\omega)$ [see Eq. (3c)] has to be performed. This, in turn, requires knowledge of the density of states $\rho(\hbar\omega)$ in the full range of ω including the correct limits for $\omega \to \infty$. Since our estimates of Eq. (11) are only good in a restricted frequency range, such a calculation is impossible in our case. Thus, a numerical computation of $\rho(E)$ is required. This lies outside the scope of the present treatment, but we hope that the detailed experimental information of Table I will stimulate theoretical work in this area. Table I, however, shows an increase in $|\delta\Omega|$ with increasing carrier concentration, in qualitative agreement with the tendencies found for Γ and the mutual relationship of these two parameters through Eq. (3c).

Finally, in Table II, we show the parameters resulting from fitting experimental curves on selected samples at room temperature with the line shapes of Eqs. (2). Excellent fits were also obtained in all cases,[5] as shown in Fig. 4. These parameters show the same trends as their counterparts from Table I: We find values of $\eta = (\Gamma^3 q^2)^{1/5}$ and $\beta = q(4880)/q(6471)$ which are constant regardless of the carrier concentration (with the exception of the pathological sample with $p = 4\times10^{20}$ cm^{-3}). Also, values of Γ and $\delta\Omega$ are found which, for a given carrier concentration, do not depend on the scattering frequency. It is interesting to observe

TABLE II. Parameters obtained from fitting experimental first-order Raman spectra of p-type Si at $T = 300$ K for two different scattering wavelengths. ($\lambda_L = 4880$ and $\lambda_L = 6471$ Å) with Eqs. (2). The values of η are computed for $\lambda_L = 4880$ Å.

$10^{-19} N$ (cm^{-3})	q $\lambda_L = 4880$ Å	q $\lambda_L = 6471$ Å	Γ (cm^{-1}) $\lambda_L = 4880$ Å	Γ (cm^{-1}) $\lambda_L = 6471$ Å	$\delta\Omega$ (cm^{-1}) $\lambda_L = 4880$ Å	$\delta\Omega$ (cm^{-1}) $\lambda_L = 6471$ Å	$\eta = (\Gamma^3 q^2)^{1/5}$ (cm$^{-3/5}$)	$q(4880)/q(6471)$
7.0	8.8	3.9	5.6	5.6	−2.0	−2.0	6.7	2.3
16	5.1	2.0	8.2	8.2	−4.9	−4.9	6.8	2.6
40	3.2	0.65	11.4	12.1	−11.9	−11.7	7.0	4.9

what changes temperature produces on the parameters of the fit. For this purpose we list in Table III the ratios of these parameters at room and liquid-nitrogen temperatures: Γ and η are seen to increase with increasing temperature, while $\delta\Omega$ and β show the opposite trend. Only a rough qualitative discussion of these trends is possible at the present level of our theoretical formulations for Γ, $\delta\Omega$, and q. From Eq. (10) we see that Γ depends on temperature through two factors: the Bose factors giving the phonon-occupation numbers and through $\rho(E)$, which depends on temperature through its dependence on the Fermi energy. At very high carrier concentrations the Fermi energy practically does not change from 77 to 300 K (since the high value of μ makes it already degenerate at room temperature). Therefore, the temperature dependence of Γ should come merely from the Bose factor of Eq. (10) which predicts:

$$(1+n_B)_{T=300\ \mathrm{K}}/(1+n_B)_{T=77\ \mathrm{K}} = 1.09\ .$$

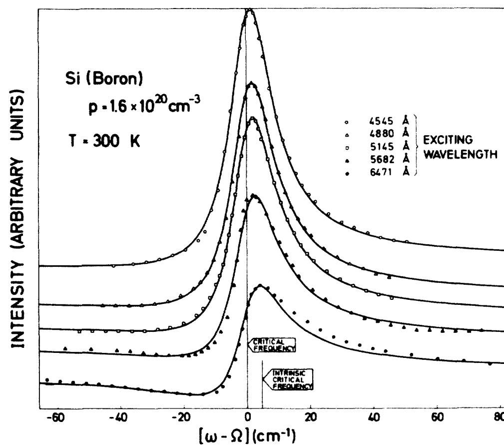

FIG. 4. Room-temperature Raman line shapes vs scattering wavelength for p-Si. The solid lines are theoretical fits, with Eq. (2), to the experimental lines (discrete points). The curves have been shifted vertically with respect to each other, with the antiresonance minimum in each case defining the base line. The critical energy is the same for all curves. The relative heights of the different curves are the ones found experimentally.

We see that this prediction agrees well with the value found experimentally for $\Gamma(300)/\Gamma(77)$ in the sample with the highest concentration of carriers (4×10^{20} cm^{-3}). As the carrier concentration decreases, we expect considerable deviations from this number owing to the stronger temperature dependence of $\rho(E)$. This prediction is borne out in Table III. Likewise the carrier-concentration-independent parameter $\eta = (\Gamma^3 q^2)^{1/5}$ should depend on temperature only through the Bose factors. The values listed in Table III are consistent with this interpretation.

More difficult to interpret are the changes in $\delta\Omega$ and β with temperature. In the latter case, one would expect the same temperature dependence as for the parameter η since both are essentially carrier-concentration independent. It is difficult, however, to pinpoint the temperature dependence of β since only three carrier concentrations were measured, and the parameter q is the one obtained with the greatest error from the fit. In view of this error, the observed dependence of Table III can be regarded as consistent with our previous considerations. Finally, the dependence of $\delta\Omega$ on temperature cannot be accounted for without analytic expressions giving the carrier concentration dependence of this quantity. However, it is interesting to note that this dependence is in qualitative agreement with the temperature dependence of δC_{44} discussed in our previous paper.[3] The sign of $\delta\Omega$ ($\delta\Omega < 0$) is also in qualitative agreement with the measured changes in C_{44} ($\delta C_{44} < 0$). This suggests the existence of a link between these two quantities (perhaps analogous to the link found in the case of

TABLE III. Ratio between the parameters of the Fano line shape fits of Tables I and II at room and at liquid-nitrogen temperatures. Here $\beta = q(4880)/q(6471)$.

$10^{-19} N$ (cm^{-3})	$\Gamma(300)/\Gamma(77)$	$\delta\Omega(300)/\delta\Omega(77)$	$\beta(300)/\beta(77)$	$\eta(300)/\eta(77)$
7.0	0.92	1.08	1.53	1.20
16	1.01	0.75	1.00	1.15
40	1.11	0.80	0.71	1.10

Ge[1]). The dependence of both effects on uniaxial stress, to be discussed in Sec. IV B, evokes even closer links, the theoretical implications of which should be of interest in clarifying the nature of the electron-phonon interaction in heavily doped semiconductors.

B. Under [001] Uniaxial Stress

The application of uniaxial stress splits the Γ_8 states at the top of the valence band.[14,17] At high enough stresses, and for low doping, it is possible to separate both bands sufficiently so that all carriers are left in one band. With increasing stress the low-energy cutoff of the inter-valence-band continuum moves to higher energies and eventually ceases to overlap with the discrete one-phonon state. Thus, the Fano discrete-continuum interaction disappears upon application of sufficiently high uniaxial stress. Before this limit is reached we would expect a gradual decrease of the effects reported in Sec. IV A as a function of uniaxial stress, i.e., we expect an increase in q and a decrease in Γ as the stress increases. Also, the uniaxial stress splits the line into a singlet (Ω_s) and a doublet (Ω_d) corresponding to phonon polarizations parallel or perpendicular to the stress axis, respectively.[12,13] Symmetry considerations predict different behavior in the stress dependence of $\delta\Omega$, Γ, and q for each of these lines. Quantitative predictions of this effect are extremely difficult owing to the added complications that the external stress introduces in the already complex valence-band structure of Si. However, it is relatively easy to follow qualitatively the striking developments in the Raman line shape as a function of stress. These developments show a number of similarities with our previous discussion of elastic constants,[3] which provide strong indications of the relationship between the effect of carriers in elastic constants and Raman spectrum. Some aspects of this comparison were pointed out in a preliminary report,[18] although the understanding of the Raman line shape outlined in Secs. I–IV was not available at the time. Here we present a systematic experimental investigation of the observed effects on the Raman line shape and position of heavily doped p-type Si as a function of uniaxial stress for several values of the carrier concentration. In order to analyze the results, the understanding of the line shape gained in Sec. IV A is used, by fitting the experimental line shape with the theoretical expression of Eqs. (2), in the manner previously described. From such fits the variations of the relevant parameters (Γ, $\delta\Omega$, and q) with the applied stress can be followed for a variety of doping levels. In Fig. 5 we present the room-temperature stress dependence of Γ and $\delta\Omega$ for a sample containing 7×10^{19} carrier/cm^3. The points were

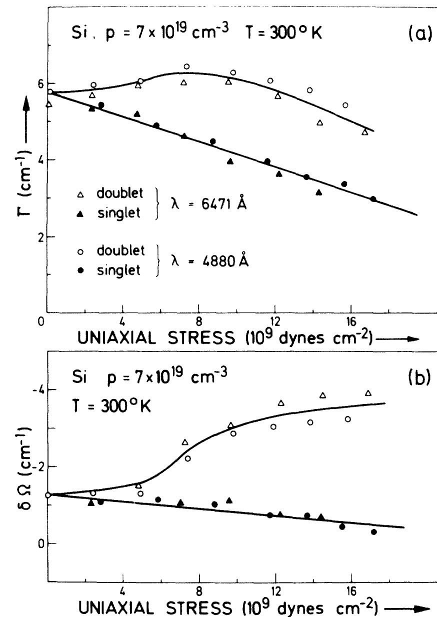

FIG. 5. Stress dependence of the parameters of the Fano fit: (a) parameter Γ vs uniaxial stress; (b) frequency shift $\delta\Omega$ vs uniaxial stress. Traingles correspond to measurements with the 6471-Å laser line while circles indicate measurements with the 4880-Å line. Open circles (triangles) represent parameters pertaining to the doublet phonon while full circles (triangles) signify the singlet. Measurements were performed on boron-doped Si with 7×10^{19} carriers/cm^3 at room temperature. The solid lines are interpolations between experimental points.

taken for two exciting wavelengths, 4880 and 6471 Å, represented by circles and triangles, respectively. Open circles (triangles) represent the parameters pertaining to the doublet lines while full circles (triangles) signify the singlet. We observe again that the parameters Γ and $\delta\Omega$ and their stress dependence are independent of the exciting frequency in full agreement with the considerations of Secs. I–III. Hence, in the future, we shall discuss results taken for only one exciting frequency. We observe that both $|\delta\Omega|$ and Γ for the doublet line show an increase with increasing stress passes through a maximum, and decreases at high stresses. In the singlet line both Γ and $|\delta\Omega|$ decrease monotonically (and indeed roughly linearly) with increasing stress. The same trends were observed in the stress dependence of δC_{44} (doublet) and δC_{66} (singlet) discussed in Ref. 3. In Fig. 6 we present the dependence of q^{-1} for both singlet and doublet lines taken with two different exciting lines (6471 and 4880 Å). A marked dependence of q and its stress dependence on the frequency of the exciting line is found, as expected from the con-

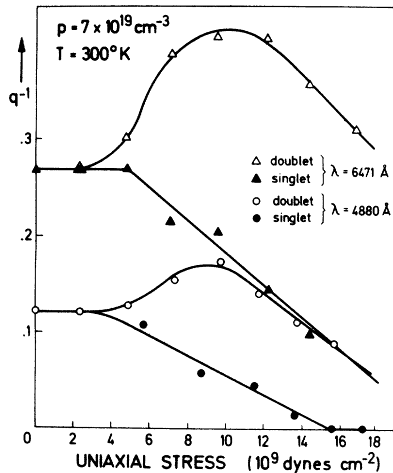

FIG. 6. Parameter q from the Fano fit vs uniaxial stress, for boron-doped Si with $p=7\times10^{19}$ cm^{-3} at $T=300$ K. Triangles and circles indicate measurements with the 6471- and 4880-Å laser lines, respectively. Open circles (triangles) indicate doublet phonon while full circles (triangles) signify the singlet. The continuous line is an interpolation between the experimental points.

siderations of Sec. IV A. Again, we observe that the singlet shows a monotonic decrease in q^{-1} (the line becomes more symmetric) while in the doublet this quantity initially increases, passes through a maximum and decreases at very large stresses. A simple argument (see Appendix B) shows that application of stress makes the electronic transitions of the overlapping continuum more probable for the electric field polarizations leading to doublet scattering as for those leading to singlet scattering. Indeed, we find at sufficiently high stresses the relationship, for a given carrier concentration and exciting frequency;

$$\frac{q(\text{singlet})}{q(\text{doublet})} \sim 2\left[\frac{\Gamma(\text{doublet})}{\Gamma(\text{singlet})}\right]^{1/2} .$$

This result is in excellent qualitative agreement with Fig. 6.

In order to reach regions where all carriers can be transferred into one band for experimentally attainable stresses, samples of low carrier concentrations must be selected. Consequently, we studied the stress dependence of the Raman spectrum in samples with 2.6×10^{19} and 6×10^{18} carriers/cm^3. At such low doping levels the carrier-induced frequency shift $\delta\Omega$ becomes too small (approximately the experimental uncertainty) for its stress dependence to be studied. Hence, for these samples only the stress dependence of Γ was determined. In Fig. 7 this dependence is plotted for both samples. We observe that the parameter Γ for the singlet decreases linearly with stress and attains the value corresponding to the intrinsic material at the point where the lower band crosses the Fermi energy. This crossing was determined from average bands computed with a $\vec{k}\cdot\vec{p}$ Hamiltonian as explained in Ref. 3. On the other hand, the doublet shows an initial increase in Γ with increasing stress, passes through a maximum and then decreases. For the sample containing 6×10^{18} carriers/cm^3, the decrease of Γ(doublet) for very high stress X goes like X^{-1}. This is evident from Fig. 8 where Γ(doublet) is plotted versus X^{-1} for the high-stress points. It is to be noted, that the trends observed in Figs. 7 and 8 coincide exactly with those predicted and observed for the electronic contribution to the elastic constants C_{44}.[3] This similarity points again to the close relationship that exists between δC_{44} (associated with the electron-phonon interaction for zone center acoustical phonons) and its counterparts $\delta\Omega$ and Γ (associated with the corresponding optical phonons). Finally, Fig. 9 shows a plot of q^{-1} for a carrier concentration of 2.6×10^{19} cm^{-3} where a behavior similar to the one previously discussed is evident. Here the asymmetry in the Raman spectrum disappears ($q^{-1}\simeq0$) at 7×10^9 dyn cm^{-2} for the singlet, and at 15×10^9 dyn cm^{-2} for the doublet. A similar plot

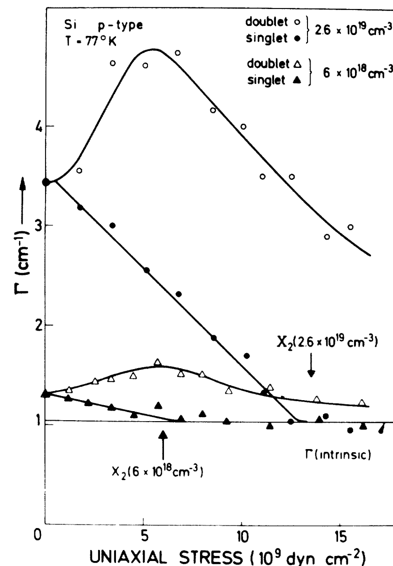

FIG. 7. Parameter Γ from the Fano fit vs stress for boron-doped Si with $p=2.6\times10^{19}$ carriers/cm^3 ($\lambda_{\text{laser}}=5145$ Å) (circles) and $p=6\times10^{18}$ carriers/cm^3 ($\lambda_{\text{laser}}=4880$ Å) (triangles). As before, open and full circles (triangles) signify doublet and singlet phonons, respectively. The arrows and the letters X_2 represent the value of the uniaxial stress for which the lower valence band crosses the Fermi energy. The measurements were performed at 77 K.

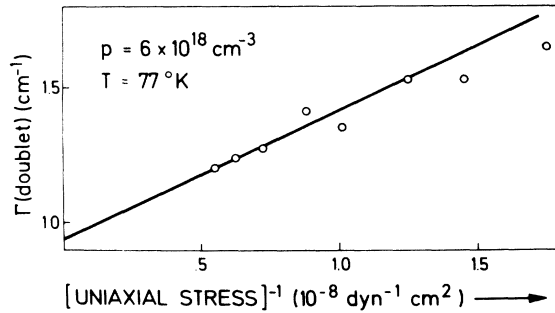

FIG. 8. Parameter Γ for the doublet phonon in a sample with $p = 6\times10^{18}$ carriers/cm^3 (open circles) vs inverse stresses (X^{-1}).

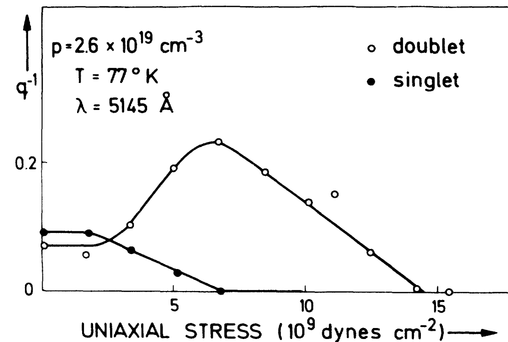

FIG. 9. Parameter q vs stress for a sample with $p = 2.6\times10^{19}$ carriers/cm^3 at $T = 77$ K with the $\lambda = 5145$-Å line of an argon-ion laser. Open (full) circles indicate the doublet (singlet) phonon line.

for the sample containing 6×10^{18} carriers/cm^3 is not shown here since $q^{-1}\simeq 0$ even at zero stress (see Table I); in this case Γ is directly the half-width of the experimental curve.

In conclusion, the stress dependence of the Raman spectrum of heavily doped Si brings out several interesting points.

(i) By studying the effect of strain on the parameters Γ, δΩ [obtained from fitting the experimental curves with the line shape of Eqs. (2)] from spectra taken at different scattering frequency we observe their independence of the latter. This gives additional proof of the soundness of the interpretation of the Raman spectrum in p-type Si presented in Secs. I–IV.

(ii) The dependence of q on strain is in agreement with its definition of Eq. (4), as the ratio of the one-phonon to the electronic Raman tensor. The fact that $q^{-1}\simeq 0$ at high stresses implies that the continuum is moved, by the stress, into energy regions where it no longer overlaps with the phonon energy.

(iii) The behavior of the parameter Γ and δΩ for high doping levels is in qualitative agreement with the stress dependence of the carrier-induced change in elastic constants discussed in Ref. 3.

(iv) At low doping levels it is found that Γ for the singlet decreases linearly with stress, attains the value of Γ found in intrinsic samples and is flat afterwards. The point at which Γ attains the intrinsic value, coincides with the crossing of the lower band through the Fermi energy (a point at which all carriers are contained in the upper band). The doublet Γ initially increases, passes through a maximum and disappears at high stresses as X^{-1}. These tendencies are surprisingly similar to those found in the stress dependence of the carrier-induced changes in the elastic constants δC_{66} (singlet) and δC_{44} (doublet) discussed in our previous paper. This emphasizes the close relationship between the carrier effects in C_{44} and those on the frequency (δΩ) and lifetimes (Γ^{-1}) of the corresponding optical phonon. The exact nature of this relationship could only be disclosed by a microscopic treatment of the electron-phonon interaction. While such a treatment lies outside the scope of the present work, we hope that the detailed experimental study presented here, will stimulate theoretical research in this area.

ACKNOWLEDGMENTS

The authors are grateful to Dr. Hilda A. Gomez de Cerdeira for many fruitful discussions and helpful suggestions concerning the theoretical interpretation of our results.

APPENDIX A

At sufficiently large k's ($\mu > \frac{2}{3}\Delta_0$) the valence-band wave function can be represented for symmetry directions in $\vec{k}$ space by[3,9,14]

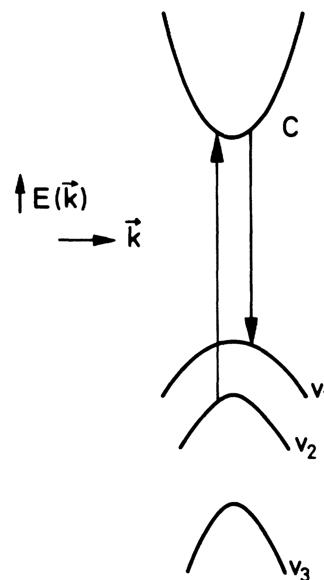

FIG. 10. Valence band and first conduction band of Si under [001] uniaxial stress.

TABLE IV. Matrix element of the electron-phonon interaction for different symmetry directions in $\vec{k}$ space in the deformation potential approximation.

Direction	Multiplicity	$\bar{X}$	$\bar{Y}$	$\bar{Z}$	$\langle \nu_1 \mid H \mid \nu_2 \rangle$
[001]	6	X	Y	Z	$\frac{1}{2}\,\delta E$
[111]	2	$\sqrt{\frac{1}{2}}\,(X-Y)$	$\sqrt{\frac{1}{6}}\,(X+Y-2Z)$	$\sqrt{\frac{1}{3}}\,(X+Y+Z)$	0
[$\bar{1}$11]	6	$\sqrt{\frac{1}{2}}\,(Y-Z)$	$\sqrt{\frac{1}{6}}\,(2X+Y+Z)$	$\sqrt{\frac{1}{3}}\,(-X+Y+Z)$	$\frac{4}{3}\,(\frac{1}{2}\,\delta E)$
[110]	6	$\sqrt{\frac{1}{2}}\,(-X+Y)$	Z	$\sqrt{\frac{1}{2}}\,(X+Y)$	$-\frac{1}{2}\,(\frac{1}{2}\,\delta E)$
[1$\bar{1}$0]	6	$\sqrt{\frac{1}{3}}\,(X+Y+Z)$	$\sqrt{\frac{1}{6}}\,(X+Y-2Z)$	$\sqrt{\frac{1}{2}}\,(X-Y)$	$-\frac{3}{2}(\frac{1}{2}\,\delta E)$

$$| \nu_1 \rangle = \sqrt{\tfrac{1}{2}}\,(\bar{X}+i\bar{Y})\uparrow, \quad | \nu_2 \rangle = \sqrt{\tfrac{1}{2}}\,(\bar{X}-i\bar{Y})\uparrow \,, \tag{A1}$$

and their corresponding time-reversed partners. Here the $\bar{Z}$ axis corresponds to the direction of the wave vector $\vec{k}$, $\bar{X}$ lies along a direction perpendicular to the plane defined by the wave vector $\vec{k}$ and the polarization of the phonon, and $\bar{Y}$ lies on a direction which is perpendicular to both $\bar{X}$ and $\bar{Z}$. We denote the crystallographic axis by X, Y, and Z. Denoting the electron-phonon interaction in the deformation potential approximation by H_ρ we get[9]

$$\langle X | H_\rho | Y \rangle = \langle X | H_\rho | Z \rangle = \langle Y | H_\rho | Z \rangle = \tfrac{1}{2}\delta E \,, \tag{A2}$$

all other matrix elements = 0 .
Here δE is the splitting of the top of the valence-band produced by the zone-center optical phonon whose polarization was arbitrarily chosen to be along the [111] axis (all polarizations being equivalent in a diamond-type material). Using Eq. (A1) we obtain

$$\langle \nu_1 | H_\rho | \nu_2 \rangle = -\tfrac{1}{2}[\langle \bar{X} | H_\rho | \bar{X} \rangle - \langle \bar{Y} | H_\rho | \bar{Y} \rangle] + i \langle \bar{X} | H_\rho | \bar{Y} \rangle \,. \tag{A3}$$

It is now straightforward to calculate the matrix element of Eq. (A3) for different symmetry directions in $\vec{k}$ space. The results are listed in Table IV from which we obtain the average matrix element,

$$\langle | \langle \nu_1 | H_\rho | \nu_2 \rangle |^2 \rangle_{\rm av} = \tfrac{95}{78}\,(\tfrac{1}{2}\,\delta E)^2 \quad . \tag{A4}$$

APPENDIX B

For sufficiently high uniaxial stress the band structure of Si near $\vec{k}=0$ is illustrated in Fig. 10. We focus our attention on transitions from the bands 1 and 2 to the conduction band, since the split-off band contains always less than 4% of the carrier.[3] The wave functions for these two bands have the same symmetry as

$$| \nu_1 \rangle = \sqrt{\tfrac{2}{3}}\, Z\uparrow - \sqrt{\tfrac{1}{6}}\,(X+iY)\downarrow, \quad | \nu_2 \rangle = -\sqrt{\tfrac{1}{2}}\,(X+iY)\uparrow \,, \tag{B1}$$

and their respective time conjugated partners. Here X, Y, and Z refer to the crystallographic axes and the arrow corresponds to spin up or down. The conduction band has the symmetry of X, Y, and Z. The dipole moment matrix element entering into the Raman intensity of the relevant electronic transition (see Fig. 10) is given by

$$| P |^2 = \sum_{\alpha \neq \alpha', c} | \langle \nu_\alpha | \vec{E}_s | c \rangle \langle c | \vec{E}_i | \nu_{\alpha'} \rangle |^2 , \tag{B2}$$

where α and α' are indices covering all valence-band states, c runs over all conduction-band states, and $\vec{E}_s$ and $\vec{E}_i$ are the polarization vectors of the scattered and incident radiation. We have

$$E_s = E_i = \sqrt{\tfrac{1}{2}}\,(X-Y) \tag{B3}$$

for the doublet and

$$E_i = Z, \quad E_s = \sqrt{\tfrac{1}{2}}\,(X-Y) \tag{B4}$$

for the singlet. Using the fact that

$$| \langle X_i | X_j | X_k \rangle | = | Q e_{ijk} | \,, \tag{B5}$$

where e_{ijk} is the Levichevita tensor, and i, j, k denote the crystallographic axes, we obtain

$$\text{singlet} \quad | P |^2 = \tfrac{1}{6}\, | Q |^4 \,,$$

$$\text{doublet} \quad | P |^2 = \tfrac{2}{3}\, | Q |^4 \,.$$

Hence, we have

$$| R_e(\text{doublet}) |^2 / | R_e(\text{singlet}) |^2 = 4. \tag{B6}$$

[1]F. Cerdeira and M. Cardona, Phys. Rev. B **5**, 1440 (1972).
[2]R. W. Keyes, in *Solid State Physics*, edited by F. Seitz and D. Turnbull (Academic, New York, 1967), Vol. 20, p. 37.
[3]T. A. Fjeldly, F. Cerdeira, and M. Cardona, preceding paper Phys. Rev. B 8, 4723 (1973).
[4]R. Beserman, M. Jouanne and M. Balkanski, in *Proceedings of the Eleventh International Conference on the Physics of Semiconductors, Warsaw 1972* (PWN-Polish Scientific, Warsaw, 1972), p. 1181.
[5]F. Cerdeira, T. A. Fjeldly, and M. Cardona, Solid State Commun. 13, 325 (1973).
[6]U. Fano, Phys. Rev. **124**, 1866 (1961).
[7]R. Braunstein and E. O. Kane, J. Phys. Chem. Solids **23**, 1423 (1962).
[8]E. Merzbacher, *Quantum Mechanics* (Wiley, New York, 1961), p. 152.
[9]F. Cerdeira, Ph.D. thesis (Brown University, 1972) (unpublished).
[10]B. A. Weinstein and M. Cardona (unpublished).
[11]J. C. Hensel and G. Feher, Phys. Rev. **129**, 1041 (1963).

[12]E. Anastassakis, A. Pinczuk, E. Burstein, F. H. Pollak, and M. Cardona, Solid State Commun. **8**, 133 (1970).
[13]F. Cerdeira, C. J. Buchenauer, F. H. Pollak, and M. Cardona, Phys. Rev. B **5**, 580 (1972).
[14]F. H. Pollak and M. Cardona, Phys. Rev. **172**, 816 (1968).
[15]R. Haensel, G. Keitel, C. Kunz, and P. Schreiber, Phys. Rev. Lett. **25**, 208 (1970).
[16]D. L. Rousseau and S. P. S. Porto, Phys. Rev. Lett. **20**, 1354 (1968).
[17]L. D. Laude, F. H. Pollak, and M. Cardona, Phys. Rev. B **3**, 2623 (1969).
[18]T. A. Fjeldly, F. Cerdeira, and M. Cardona, Solid State Commun. **12**, 553 (1973).